Electronic Supplementary Material (ESI) for Journal of Materials Chemistry A.

Supplementary Information

p-type SnO Thin Layers on *n*-type SnS_2 Nanosheets with Enriched Surface Defects and Embedded Charge Transfer for the Lithium Ion Battery

Yiqiong Zhang, Zhaoling Ma, Dongdong Liu, Shuo Dou, Ming Zhang, Jianmin Ma, Zaiping Guo, Ru Chen and Shuangyin Wang**

*E-mail: shuangyinwang@hnu.edu.cn

Experimential section

Material Preparation.

The SnS_2 nanosheets grown on carbon paper were synthesized by a facile solvothermal method. In a typical process, the carbon paper was pretreated in a muffle furnace to remove the surface impurities. Next, 0.35 g tin chloride pentahydrate and 0.40 g thioacetamide were dissolved in 40 mL ethanol under magnetic stirring for 2 h. After that, the carbon paper was immersed in the mixed solution and transferred to a 50 mL autoclave, sealed and kept in an oven at 160 ^oC for 12 h. The product was obtained and washed with deionized water and ethanol, and dried at 60 ^oC under vacuum overnight. The mass loading of SnS_2 on carbon paper was around 2.5 mg cm^{-2}. The SnS_2 nanosheet grown on carbon paper was treated by Ar plasma (13.56 MHz) with power of 150 W and pressure of 50 Pa for different irradiation time: 0 min, 5 min, 10 min, 15 min, and 30 min. And then, the plasma treated samples were taken out from the plasma tube reactor and exposed to air overnight. The samples which treated at 0 min and 10min were noted as SnS_2 and SnS_2/SnO, respectively.

Material Characterizations.

The X-ray diffraction (XRD) measurements used a Rigaku D/MAX 2500 diffractometer with Cu Kα radiation. The Raman spectra were collected on a Raman spectrometer (Labram-010) using 532 nm laser. The morphology and microstructure of the SnS_2 and SnS_2/SnO were investigated by scanning electron microscope (SEM, Hitachi, S-4800) and transmission electron microscope (TEM, FEI, F20 S-TWIX). The X-ray photoelectron spectroscopic (XPS) measurements were carried out with an ESCALAB 250Xi using a monochromic Al X-ray source (200 W, 20 eV). The nitrogen adsorption-desorption isotherms were measured at 77 K with a Quantachrom NOVA 1000e system.

Electrochemical Measurements.

The electrochemical characteristics of the synthesized samples were evaluated by using half cells (2032 coin cell). The cells were assembled in an Ar-filled glovebox. Li foils served as the counter electrode and reference electrode, and the electrolyte was a 1.0 M $LiPF_6$ solution in a mixture of ethylene carbonate/dimethyl carbonate (EC/DMC) (1:1 in volume), and a polypropylene film (Celgard-2400) was used as a separator. The working electrodes were prepared by cutting the carbon paper which covered uniformly with the samples into smaller disks with the diameter of 12 mm. The galvanostatic charge/discharge cycles were carried out on a Land CT2001A battery tester between 0.001 and 3.00 V at various current densities. Electrochemical impedance spectroscopy and cycle voltammetry were conducted on a PGSTAT 302N electrochemical workstation at a scan rate of 0.1 mV s^{-1}. At least five parallel cells were tested for each electrochemical measurement, in order to make sure that the results were reliable and represented the typical behavior of the samples.

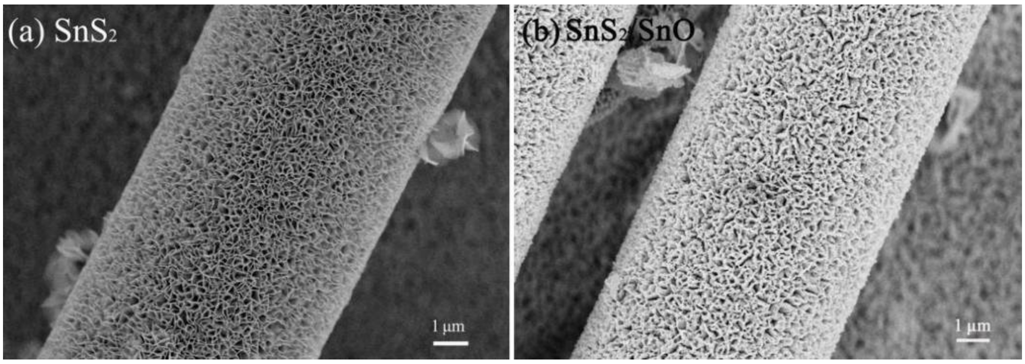

Figure S1. Low resolution SEM images of (a) SnS_2 and (b) SnS_2/SnO obtained by plasma treatment for 10 min.

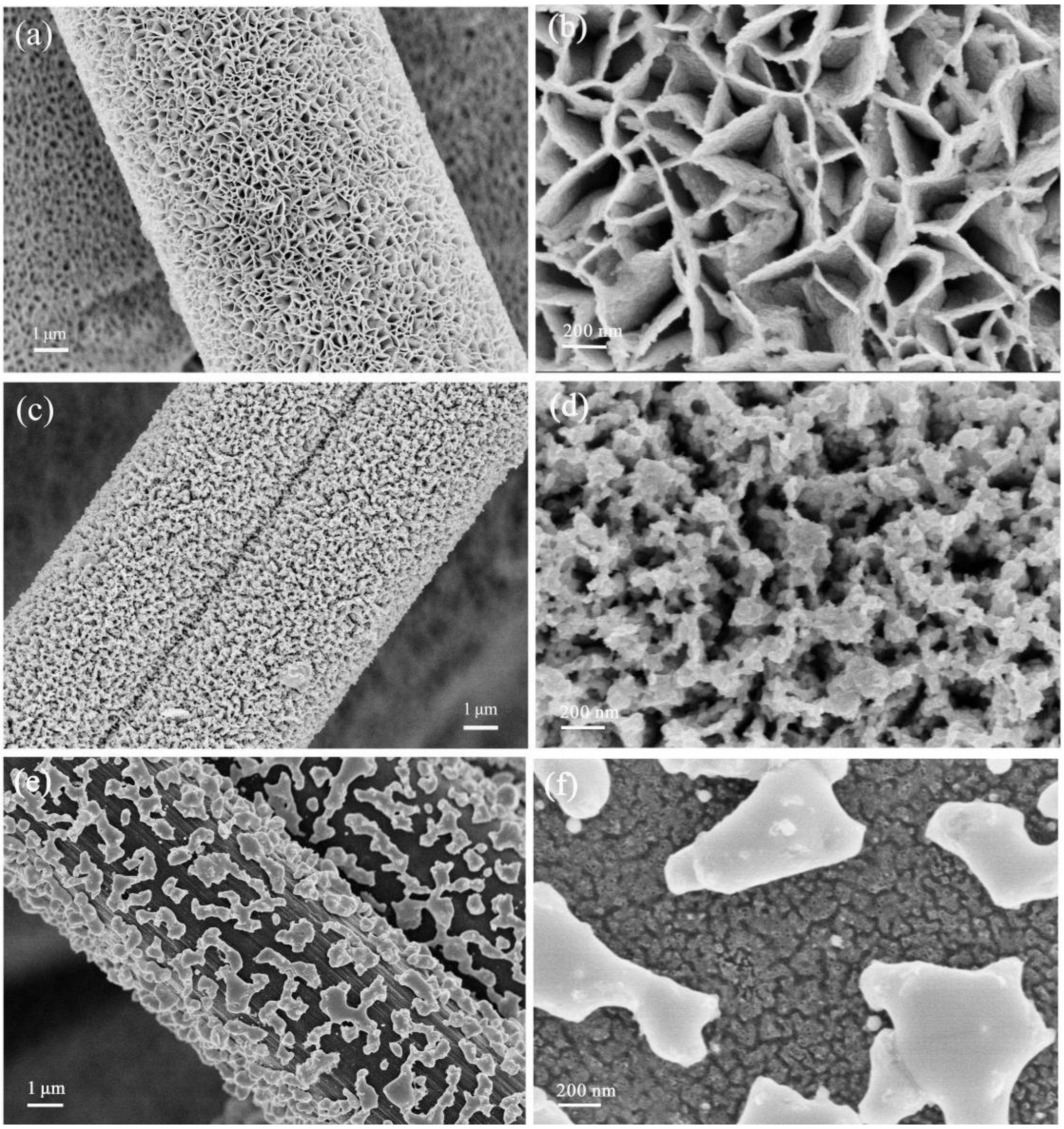

Figure S2. SEM images of the plasma treated samples for (a) and (b) 5 min, (c) and (d) 15 min and (e) and (f) 30 min. After Ar plasma treatment for 5 min, the nanosheets were slightly transformed to stacked nanoparticles, while the nanosheets treated for 15 min show serious particle aggregation. The longer treatment time of 30 min even results in the removal of the Sn-based species from the carbon fibers.

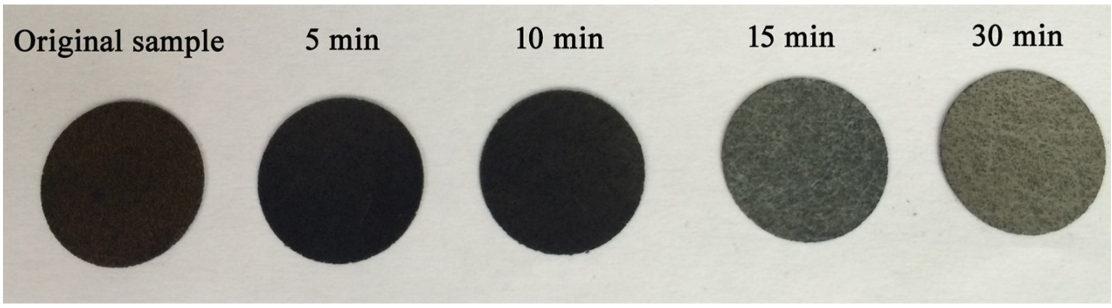

Figure S3. The macroscale carbon paper cells of different plasma irradiation time.

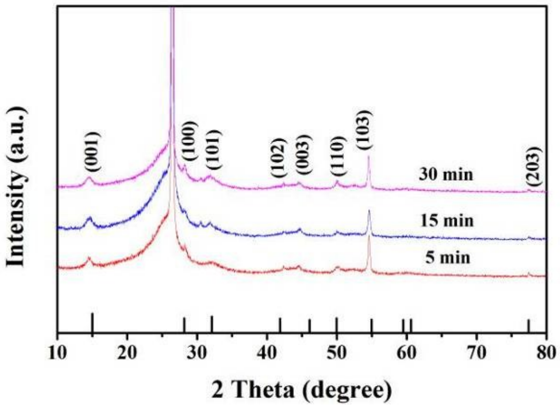

Figure S4. X-ray diffraction patterns of plasma-treated SnS_2 for 5 min, 15 min and 30 min. A peak at 29.8° for both samples after plasma-treatment for 15 min and 30 min is indexed to the SnO phase (101) with a romarchite structure (*JCPDS Card no.06-0395*).

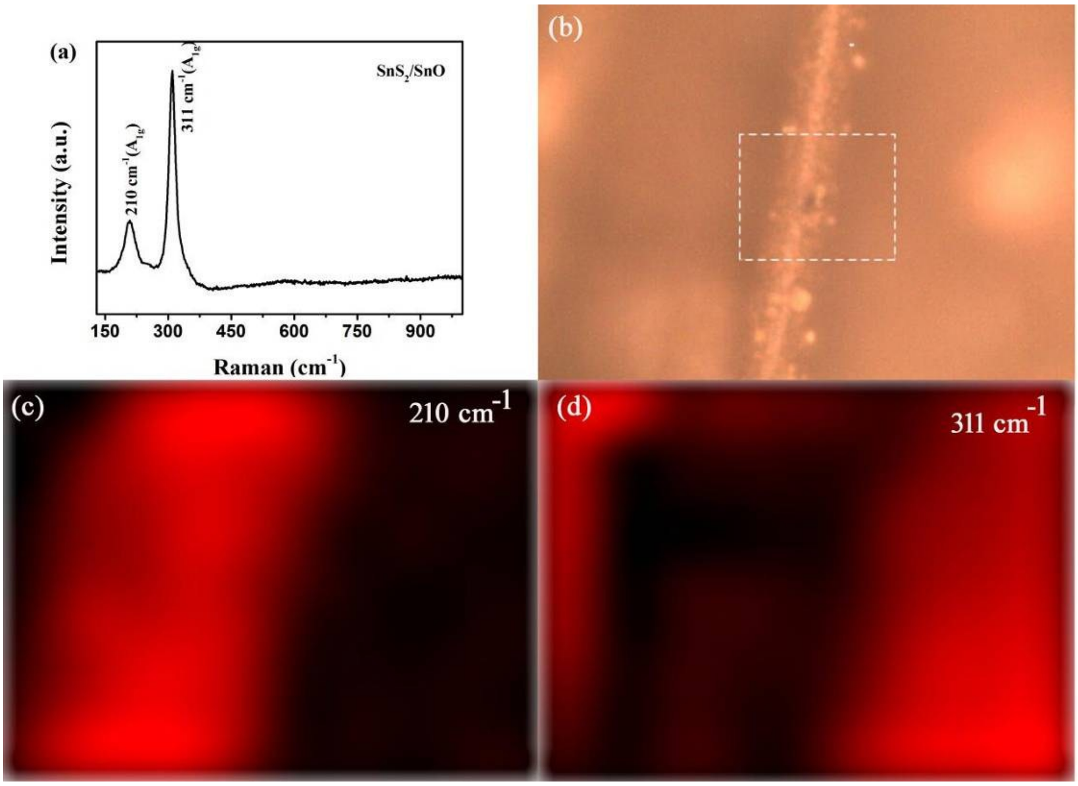

Figure S5. Raman mapping of SnS$_2$/SnO, which further confirming uniform coverage of *p*-type SnO over the *n*-type SnS$_2$ surface.

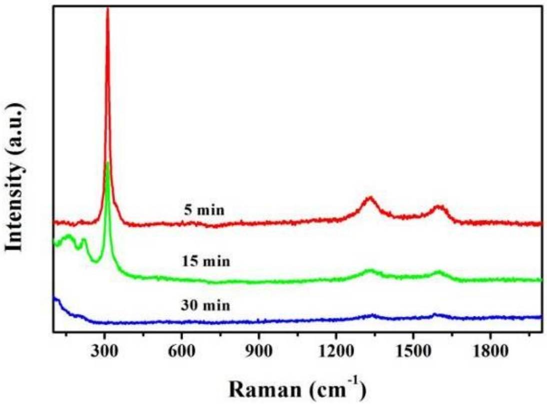

Figure S6. The Raman spectra of SnS$_2$ treated by Ar plasma for 5 min, 15 min, and 30 min. After 5 min, no SnO signals were detected. After 15 min, SnO signals were detected as they were after 10 min. More interestingly, after 30 min, all of the signals from the Sn-based materials are fully suppressed due to the removal of the Sn species from the carbon substrate

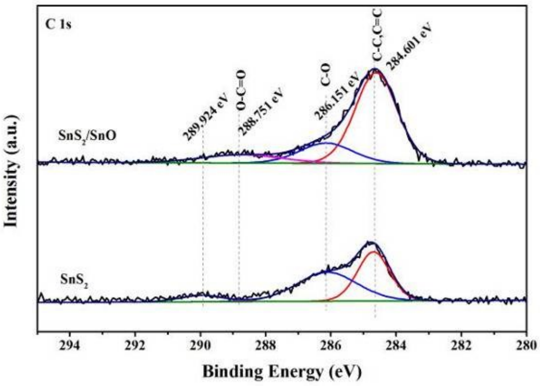

Figure S7. C 1s region XPS spectra of SnS_2 and SnS_2/SnO supported on carbon fibers.

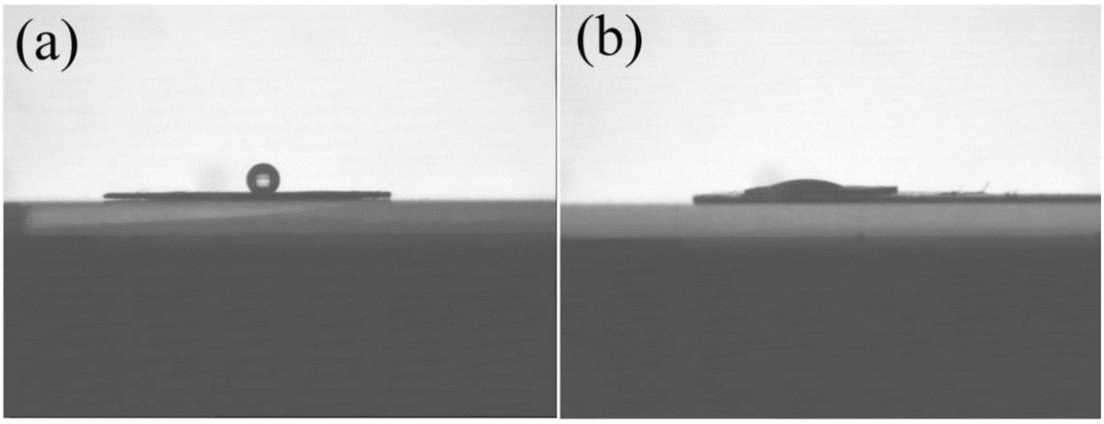

Figure S8. Contact angle measurement on (a) SnS_2 and (b) SnS_2/SnO. Compared with the SnS_2, the SnS_2/SnO treated with Ar plasma has better wettability, indicating that the SnS_2/SnO is enriched in surface defects and oxide heterostructures

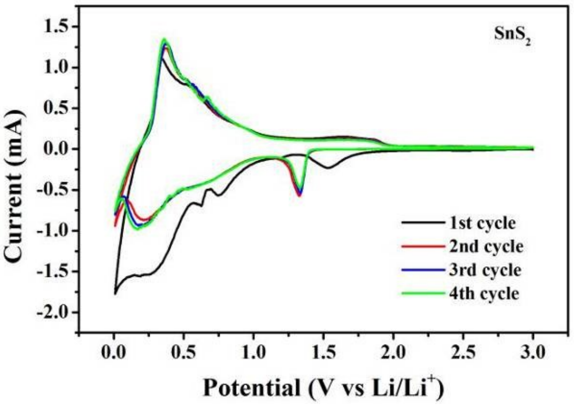

Figure S9. Cyclic voltammograms for the first four cycles of the SnS_2 electrode from 0.001 to 3 V vs Li/Li$^+$ at 0.1 mV s^{-1}.

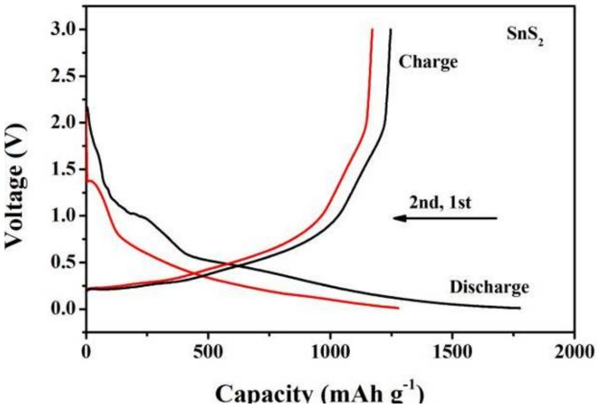

Figure S10. Galvanostatic discharge-charge profiles of SnS$_2$ electrode at a current density of 200 mA g^{-1}.

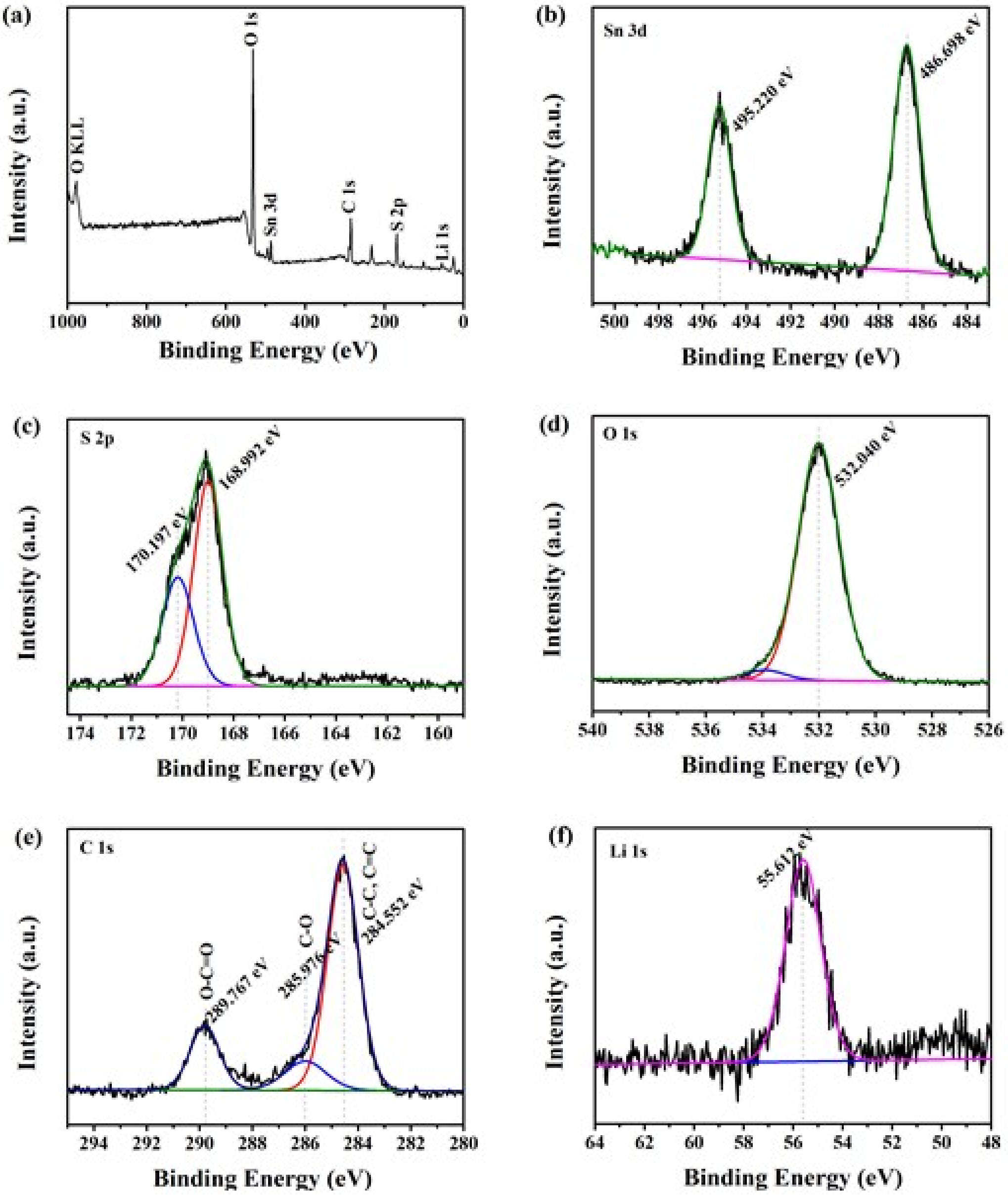

Figure S11. To determine chemical compositions of the SEI layer on the electrode, the SnS_2/SnO electrode after 50 cycles were examined by XPS, (a) XPS survey spectra, (b) After 50 cycles, the decrease of the Sn 3d peaks revealed that surface coverage of the SEI layer and the SEI layer gradually becomes thick. (c) the peak of S 2p at a binding energy of 168.992 eV and 170.197 eV was assigned to metal sulfate, (d) Before the cycling test, the O 1s peaks at binding energies of 530.741 eV and 532.041 eV in Figure 3f are attributed to the Sn-O and absorbed hydroxyl groups on the surface, respectively, After 50 cycles, the peaks shifted to higher binding energies of 532.040 eV and 533.980 eV, which could be attributed to Li_2CO_3 or carbonate in the SEI layer. (e) the peak of C 1s at a binding energy of 284.552 eV was assigned to C-H bonding of carbonate and hydrocarbon contamination. The peaks observed at binding energies of 285.976 eV and 289.767 eV were corresponded to carbon atom bound to one and two oxygen atoms, respectively, and (f) The peak intensity at a binding energy of 55.612 eV of lithium is relatively weak, therefore, it is difficult to determine the compositions.

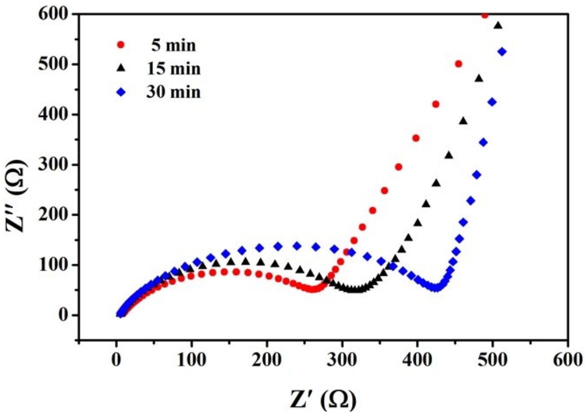

Figure S12. The Nyquist plots about the different plasma irradiation time of SnS_2 (the plasma treated for 5 min, 15 min, and 30 min). The charge transfer resistance of 5 min, 15 min and 30 min is 287, 330 and 458 Ω, respectively, much higher than that of SnS_2/SnO (109 Ω), indicating that the SnS_2/SnO have the stable structure with more surface defects can directly enhance the ions intercalation and charge transfer.

Table S1. Comparison of electrochemical performance of SnS_2/SnO in this work with previously reported materials Sn-based anodes for lithium ion batteries.

Sample	Cycling stability				Rate capability		Ref.
	Current density	Initial discapacity mA h g^{-1}	Cycle number	Capacity retention mA h g^{-1}	Current density	Capacity retention mA h g^{-1}	
SnS_2/SnO	**200 mA g^{-1}**	**1496**	**200**	**998**	**800 mA g^{-1}**	**760**	**This work**
U-SnO_x/C	500 mA g^{-1}	1278	200	608	1.0 A g^{-1}	518	**1**
SnS_2/G	1.6 mA cm^{-2} (charge) 0.2 mA cm^{-2} (discharge)	864	100	704	1.6 mA cm^{-2}	546	**2**
SnS_2/GNS-RS	0.1 C $C_{(Theoretical)}$ =591 mA h g^{-1}	1724	50	577	1 C	200	**3**
SnS_2/SnO_2/C	100 mA g^{-1}	1066	30	638	1 C (1000 mA g^{-1})	550	**4**
N-C@SnO_2/SnS/GN	100 mA g^{-1}	1970	110	1236	800 mA g^{-1}	650	**5**
Gr-SnO_2-C	200 mA g^{-1}	1310	150	757	—	—	**6**
G-SnO	44 mA g^{-1}	1451	30	485	200 mA g^{-1}	467	**7**
SnS_2@PANI	100 mA g^{-1}	1395.8	80	730.8	5000 mA g^{-1}	356.1	**8**
Sn/SnO_x	30 mA g^{-1}	1192	40	510	90 mA g^{-1}	434	**9**
α-Fe_2O_3/SnO_2	1000 mA g^{-1}	1167	30	~200	—	—	**10**
Sn/SnO_2/CNF@C	800 mA g^{-1}	1676	200	712	4.0 A g^{-1}	397	**11**
SnO_x/graphene/carbon fiber	200 mA g^{-1}	1272	480	600	1000 mA g^{-1}	504	**12**
SnO_x/CNF/CNT	500 mA g^{-1}	~900	—	—	2.0 A g^{-1}	405	**13**
SnS_2@GF	100 mA g^{-1}	1386	500	818	1.0 A g^{-1}	860	**14**

References:

1. X. Zhou, Z. Dai, S. Liu, J. Bao and Y. G. Guo, *Adv. Mater.*, 2014, **26**, 3943-3949.
2. S. Liu, X. Lu, J. Xie, G. Cao, T. Zhu and X. Zhao, *ACS applied materials & interfaces*, 2013, **5**, 1588-1595.
3. M. Sathish, S. Mitani, T. Tomai and I. Honma, *The Journal of Physical Chemistry C*, 2012, **116**, 12475-12481.
4. C.-Y. Chen, T. Yokoshima, H. Nara, T. Momma and T. Osaka, *Electrochim. Acta*, 2015, **183**, 78-84.
5. J. Shan, Y. Liu, P. Liu, Y. Huang, Y. Su, D. Wu and X. Feng, *Journal of Materials Chemistry A*, 2015, **3**, 24148-24154.
6. C. Zhang, X. Peng, Z. Guo, C. Cai, Z. Chen, D. Wexler, S. Li and H. Liu, *Carbon*, 2012, **50**, 1897-1903.
7. W. Yue, S. Yang, Y. Ren and X. Yang, *Electrochimica Acta*, 2013, **92**, 412-420.
8. G. Wang, J. Peng, L. Zhang, J. Zhang, B. Dai, M. Zhu, L. Xia and F. Yu, *Journal of Materials Chemistry A*, 2015, **3**, 3659-3666.
9. L. Zou, L. Gan, R. Lv, M. Wang, Z.-h. Huang, F. Kang and W. Shen, *Carbon*, 2011, **49**, 89-95.
10. W. Zhou, C. Cheng, J. Liu, Y. Y. Tay, J. Jiang, X. Jia, J. Zhang, H. Gong, H. H. Hng and T. Yu, *Adv. Funct. Mater.*, 2011, **21**, 2439-2445.
11. Z. Shen, Y. Hu, Y. Chen, R. Chen, X. He, X. Zhang, H. Shao and Y. Zhang, *Electrochim. Acta*, 2016, **188**, 661-670.
12. F. Yan, X. Tang, Y. Wei, L. Chen, G. Cao, M. Zhang and T. Wang, *Journal of Materials Chemistry A*, 2015, **3**, 12672-12679.
13. B. Zhang, J. Huang and J. K. Kim, *Adv. Funct. Mater.*, 2015, **25**, 5222-5228.
14. Y. Ren, W. Lv, F. Wen, J. Xiang and Z. Liu, *Mater. Lett.*, 2016, **174**, 24-27.